Available online at www.sciencedirect.com

ScienceDirect

Ceramics International 40 (2014) 4853–4868

CERAMICS INTERNATIONAL

www.elsevier.com/locate/ceramint

Properties and residual stress distribution of plasma sprayed magnesia stabilized zirconia thermal barrier coatings

M.N. Baig[a,*], F.A. Khalid[a], F.N. Khan[a], K. Rehman[b]

[a]Faculty of Materials Science and Engineering, GIK Institute of Engineering Sciences and Technology, Topi, KPK, Pakistan
[b]Faculty of Mechanical Engineering, GIK Institute of Engineering Sciences and Technology, Topi, KPK, Pakistan

Received 6 July 2013; received in revised form 5 September 2013; accepted 8 September 2013
Available online 18 September 2013

Abstract

Thermal barrier coatings (TBCs) are employed to protect hot section components in industrial and aerospace gas turbine engines. Conventional TBCs frequently fail due to high residual stresses generated within the coating systems owing to the difference between coefficient of thermal expansion (CTE) of the substrate & deposited layers. Functionally graded-thermal barrier coatings (FG-TBCs) with gradual variation in composition and microstructure have been proposed to minimize the problem. In the present study, three different TBC systems, one duplex and two FG-TBCs, having three and five layers, respectively, were prepared by atmospheric plasma spray (APS) process on Nimonic 90 substrates using Ni-5Al as bond coat (BC) and magnesia stabilized zirconia as top coat (TC) materials. Five layers comprising the three TBC systems were also deposited separately as individual coatings to study their characteristic properties. The coatings were characterized by a scanning electron microscope. Microhardness and CTE of the individual coatings were also measured. Finite element analysis (FEA) using ANSYS 14.5 was performed to estimate the thermal residual stresses generated within the as-sprayed coating systems. The microstructure, microhardness and CTE in the five-layer FG-TBC changed gradually as compared with duplex and three-layer FG-TBC. The lowest radial, axial and shear stresses were generated in the five-layer FG-TBC compared with those of the duplex and three-layer FG-TBC. Increasing the number of layers with a gradient in composition from BC to TC having similar thickness of coatings increased the bond strength of the FG-TBCs. The bond strength of five-layer FG-TBC was found to be almost 1.5 times as high as that of the duplex TBC.

Keywords: Ni-5Al bond coat; Magnesia stabilized zirconia; Plasma spraying; Finite element analysis

1. Introduction

Thermal barrier coatings (TBCs) are widely in use now-a-days to protect internally cooled parts in high temperature areas of gas turbine engines used in power generation and jet propulsion. These coatings are applied to provide a temperature drop (~170–200 °C) between the coating surface and the component thus increasing the Turbine Entry Temperature (TET) and consequently turbine engine's efficiency. The eventual target of applying a TBC is to achieve an enhancement in the fuel efficiency by increasing the operating temperature by ~100–300 °C. The incorporation of TBC therefore increases the engine thrust up to 5% and efficiency up to 1%, respectively. TBCs also extend the life of turbine components and thereby improve engine reliability [1–8].

A TBC system is a multilayered system having a complex geometry and usually consists of four layers, (1) a Ni-based superalloy substrate, (2) a metallic bond coat (BC) with god corrosion and oxidation resistance, (3) a high temperature oxidation product formed between BC and TC known as thermally grown oxide (TGO) and (4) a low thermal conductivity ceramic top coat (TC) [9]. It has been reported that most superalloys oxidize rapidly at temperatures above 900 °C as they are unable to protect themselves from oxidation by making a diffusion barrier during initial periods of oxidation [10]. The use of an approximately 100–150 μm thick layer of a metallic BC has now become a normal practice to protect the superalloy substrate from elevated temperature oxidation and corrosion [11]. The typical BC materials used in TBCs are MCrAlY (M=Ni and/or Co) alloys, Ni–Cr–Al, Ni–Cr and Ni–Al with or without Pt modification [8,11–13]. The Ni–Al

*Corresponding author. Tel.: +92 322 5075087.
E-mail address: mnbaig8167@gmail.com (M.N. Baig).

0272-8842/$ - see front matter © 2013 Elsevier Ltd and Techna Group S.r.l. All rights reserved.
http://dx.doi.org/10.1016/j.ceramint.2013.09.035

type bond coats such as Ni–20Al and Ni–5Al are recognized for their enhanced bond strengths attributed to an exothermic reaction resulting from an extra heat of solidification associated with the partial oxidation of Ni and Al during spraying [14–16]. These coatings also find a number of other applications, e.g., for restoration of machined components, in internal combustion engine cylinders as bond coats and in boiler tubes to protect them from corrosion [15–16]. It has also been reported that Ni–5Al coatings develop a protective and adherent oxide scale when cyclically oxidized at 900 °C resulting in a reduction in weight gains of the superalloy substrates hence lowering the rate of oxidation [16]. The BC is mainly meant to improve adhesion and increase oxidation resistance by making a defensive oxide layer (a thermally grown oxide, TGO), which is frequently consisting of α-Al_2O_3 [17].

The TC is characterized by a stable phase from room temperature up to the operating temperature, low thermal conductivity usually less than 2 $W\,m^{-1}K^{-1}$, comparatively high thermal expansion coefficient (CTE) usually greater than $9\times10^{-6}\,K^{-1}$, low sintering rate, high melting point and good erosion resistance [8,10–11]. The TC layer is usually 200–250 μm in thickness and is directly attached to the BC [11]. Partially or fully stabilized zirconia by adding various oxides like Y_2O_3, CeO_2, CaO, Al_2O_3, Gd_2O_3 and MgO as stabilizers are used as TC materials owing to their low thermal conductivity and relatively good mechanical properties [8,18–19]. Among these, ZrO_2–Y_2O_3 (7–8% YSZ) is documented as an exceptional TC material for the last 30–40 years as it possesses high resistance against thermal shock, low thermal conductivity and high melting point as compared to other stabilized zirconias [10]. However, it is more expensive as compared to CaO and MgO-stabilized zirconia [8,20–21]. Zirconia stabilized with 15–24% MgO (magnesia stabilized zirconia-MSZ) is comparatively cheaper and is utilized in regions where the temperature intensity is relatively low such as in the exhaust nozzle of the jet engines [20–21]. Recently, magnesia stabilized zirconia has been investigated for its hot corrosion behavior in LiCl–Li_2O molten salt owing to its excellent chemical stability [22]. Moreover, MSZ has low thermal conductivity (1.0–1.5 W/mK), fairly comparable to YSZ which suggests that it has a huge potential to be used as TC material for suitable applications.

The two main processes used to deposit TC are air plasma spray (APS) and electron beam-physical vapor deposition (EB-PVD) whereas the BC may be deposited by various methods such as APS, EB-PVD, low pressure plasma spry (LPPS), high velocity oxy-fuel spray (HVOF) and chemical vapor deposition (CVD) [23]. However, the two main techniques used to deposit commercial TBCs are plasma spraying (PS) and EB-PVD [24–25]. Plasma sprayed coatings exhibit a typical splat-on-splat structure formed by the rapid cooling of the small droplets of molten or semi-molten particles impacting the substrate at high velocities [24].

The main problem in using a conventional TBC system consisting of an oxidation resistant BC and a low thermal conductivity heat insulating TC is its premature failure because of the delamination or spallation of the ceramic TC from the metallic BC. The large residual stresses generated during cooling from the spraying temperature at or near the interface of the deposited layers and substrate are responsible for this failure. These coatings usually spall or crack either at the interface between the substrate and coating or at the interface between the BC and TC. These residual stresses are induced due to mismatch in CTE of the substrate and BC & TC and can have a considerable effect on the properties of the deposited coating system [26–29]. These stresses can produce deformation in the coated parts resulting in cracking or spallation of the coating. Furthermore, the type or nature of residual stress may affect many of the coating properties, such as bond strength, thermal cycling and erosion resistance. Therefore, to predict life of TBCs and to understand their failure mechanisms, simulation of residual stresses is an imperative and essential aspect [29].

To reduce mismatch between the CTE of the coated layers and the substrate and to enhance the service life of the TBC system, the introduction of one or more intermediate layers with compositional gradient between the bond and top coats has been proposed. These thermal barrier systems are usually referred to as functionally graded-thermal barrier coatings (FG-TBCs) [28–33]. FG-TBCs are prepared by incorporating one or more intermediate layers between the BC and TC in such a way that there is a gradual change in the composition of the deposited layers from substrate metal to ceramic coating. Compared with duplex TBC, FG-TBCs are designed to have intermediate layers deposited by mixing the BC alloy and TC ceramic in various ratios. These layers are deposited in such a manner that the layers adjacent to the BC have a metallic matrix with ceramic inclusions and the layers adjacent to the TC have a ceramic matrix with metallic inclusions. A transition layer consisting of 50% metallic phase and 50% ceramic phase is usually deposited in the center of the FG-TBC system. The incorporation of such compositionally gradient intermediate layers are expected to reduce thermal mismatch between any two adjacent layers owing to small changes in local composition and may result in improved thermo-mechanical properties [34–35].

In the present study, Ni–5Al/ZrO_2–24MgO based duplex and functionally graded TBCs (three and five layered) having same overall thickness but varying individual layers thicknesses were deposited on Nimonic 90 substrates by air plasma spraying (APS) process. This TBC system, comprising of Nimonic 90 substrate, a Ni–5Al BC, and a ZrO_2–24MgO TC, has not been investigated previously. Five layers comprising of three TBC systems were also deposited separately as individual coatings in order to study their characteristic properties. Finite element analysis (FEA) using ANSYS 14.5 was also performed to approximate the thermal residual stresses generated within the as-sprayed coating systems. Moreover, a correlation was made between the adhesion/cohesion strength (bond strength) of the deposited TBC systems with that of the FEA results.

2. Materials and methods

The substrates used in this study were approximately 3 mm thick and 12.8 mm diameter discs of a nickel-based superalloy,

Table 1
Nominal composition of Nimonic 90.

Element	Ni	Cr	Co	Ti	Al	Fe	Others
Weight %	53	20	18	2.5	1.5	1.5	3.5

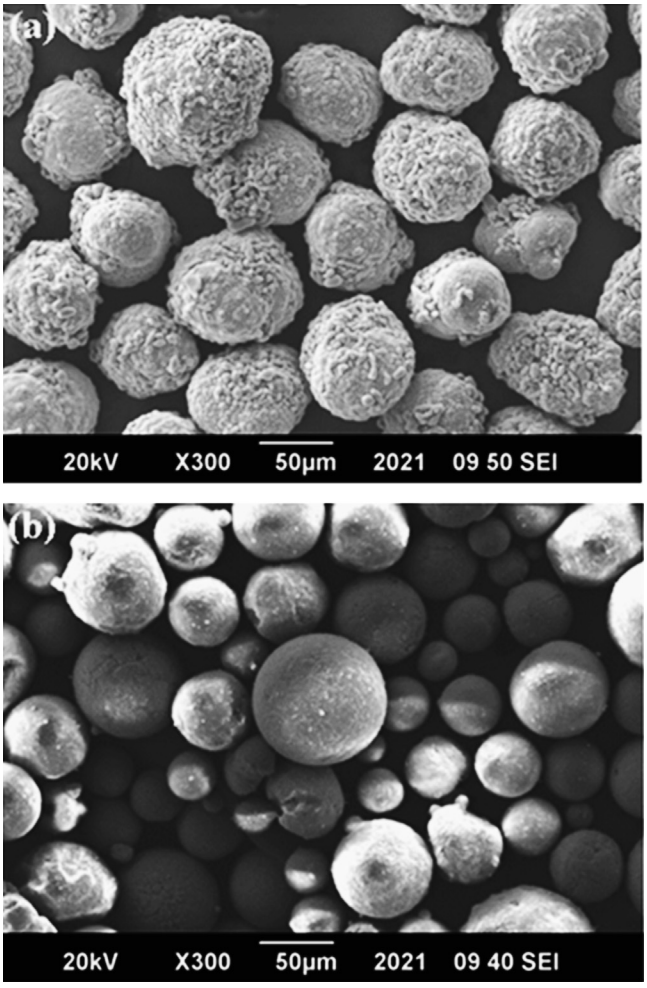

Fig. 1. SEM micrographs of feedstock powders showing morphology and particle size in, (a) Ni powder and (b) MSZ powder.

Nimonic 90, from Goodfellow Cambridge Limited, UK. The nominal composition of Nimonic 90 is given in Table 1.

Two types of commercial feedstock powders from Sulzer Metco, USA, namely Metco 450NS (Ni–5Al, will be referred as Ni in this paper), a mechanically clad and spheroidal powder having particle size distribution in the range of $-90+45$ μm and Metco 210NS-1 (ZrO_2–24MgO, will be referred as MSZ in this paper), an agglomerated and HOSP™ (Homogeneous Oven Spherical Powder Method) processed spheroidal powder having particle size distribution in the range of $-90+11$ μm, were used as BC and TC materials, respectively. SEM micrographs showing the morphology and particle size distribution of the two powders used as BC and TC materials are shown in Fig. 1(a) and (b), respectively. Both the powders showed a spheroidal morphology, however MSZ powder particles showed a perfectly round spherical

Table 2
Plasma spraying parameters used to deposit coatings.

Parameter	Limits used				
	Layer-1 (100% Ni)	Layer-2 (75Ni+25MSZ)	Layer-3 (50Ni+50MSZ)	Layer-4 (25Ni+75MSZ)	Layer-5 (100% MSZ)
Primary gas type	Ar	Ar	Ar	Ar	Ar
Primary gas pressure	690 ± 35 KPa	690 ± 35 KPa	690 ± 35 KPa	690 ± 35 KPa	690 ± 35 KPa
Primary gas flow rate	$47.2 \times 10^{-3} \pm 2.4 \times 10^{-3}$ m^3/s	$47.2 \times 10^{-3} \pm 2.4 \times 10^{-3}$ m^3/s	$47.2 \times 10^{-3} \pm 2.4 \times 10^{-3}$ m^3/s	$47.2 \times 10^{-3} \pm 2.4 \times 10^{-3}$ m^3/s	$47.2 \times 10^{-3} \pm 2.4 \times 10^{-3}$ m^3/s
Auxiliary gas type	H_2	H_2	H_2	H_2	H_2
Auxiliary gas pressure	385 ± 35 KPa	385 ± 35 KPa	385 ± 35 KPa	385 ± 35 KPa	385 ± 35 KPa
Auxiliary gas flow rate	$7 \times 10^{-3} \pm 2.4 \times 10^{-3}$ m^3/s	$7 \times 10^{-3} \pm 2.4 \times 10^{-3}$ m^3/s	$7 \times 10^{-3} \pm 2.4 \times 10^{-3}$ m^3/s	$7 \times 10^{-3} \pm 2.4 \times 10^{-3}$ m^3/s	$7 \times 10^{-3} \pm 2.4 \times 10^{-3}$ m^3/s
Powder carrier gas	Ar	Ar	Ar	Ar	Ar
Powder carrier gas flow rate	17.46×10^{-3} m^3/s	17.46×10^{-3} m^3/s	17.46×10^{-3} m^3/s	17.46×10^{-3} m^3/s	17.46×10^{-3} m^3/s
Powder feed rate	1.13 g/s	1.13 g/s	1.0 g/s	1.0 g/s	0.85 g/s
Arc current	500 Amps	500 Amps	500 Amps	500 Amps	500 Amps
Arc voltage	70 ± 5 V	70 ± 5 V	70 ± 5 V	70 ± 5 V	70 ± 5 V
Spray distance	125 mm	100 mm	100 mm	88 mm	75 mm
Anode-nozzle internal diameter	8 mm	8 mm	8 mm	8 mm	8 mm
Gun to work angle	90°	90°	90°	90°	90°

Table 3
Number of layers and thickness of duplex and FG-TBC systems.

Thickness (μm) and no. of individual layers						
TBC system	**Layer-1 (100 Ni)**	**Layer-2 (75 Ni+25 MSZ)**	**Layer-3 (50 Ni+50 MSZ)**	**Layer-4 (25 Ni+75 MSZ)**	**Layer-5 (100 MSZ)**	**Total thickness (μm)**
Duplex	100	–	–	–	200	300
Three−layer FG-TBC	75	–	75	–	150	300
Five-layer FG-TBC	50	50	50	50	100	300

morphology as compared to Ni powder particles. Surface morphologies of both the powder particles revealed that Ni particles have an irregular and rough surface whereas MSZ particles have a very smooth surface. Furthermore, SEM micrographs of both the powders demonstrated that MSZ powder has a higher range of finer size particles as compared to Ni powder.

The two powders were also pre-mixed with each other in three different ratios (by weight %) to form three powder blends, i.e., 75 Ni/25 MSZ, 50 Ni/50 MSZ, and 25 Ni/75 MSZ. These powder blends were then used to deposit functionally gradient layers in order to prepare FG-TBCs. The coatings were deposited by APS using a Metco 9MB plasma spray gun (Sulzer Metco, USA). Before depositing the coatings, the substrates were grit blasted with Corundum-500 particles to a surface roughness of ~4.0 μm, followed by ultrasonic cleaning. The plasma spray parameters used for depositing coatings are given in Table 2.

The powders and coatings were characterized by an analytical low vacuum scanning electron microscope (JEOL-Japan, Model JSM 6490 LA) operated at 20 kV and coupled with an energy dispersive spectrometer (EDS). The samples were also gold sputtered (~290 Å thick) using an ion sputtering device (JEOL-Japan, Model JFC-1500) with argon (Ar) as sputtering gas, before observing them under SEM. Microhardness profiles of the individual coatings were obtained using a Vickers Indenter (Wilson Instruments, USA, Model 401MVD) with a 300 gf (2.941995 N) load and 15 s. dwell time (loading time). The CTE of individual free-standing layers were measured as a function of temperature using a dilatometer (Netzsch Germany, model 402E). The approximate sample size was 03 × 03 × 25 mm and the heating rate was 10 °C/min. Bond strengths (adhesion/cohesion strengths) of the coatings were measured as per requirements of ASTM Standard C633-01.

Table 3 tabulates the three TBC systems prepared with each individual layer thickness and the overall thickness of each TBC system which was kept approximately same in this study for comparison. The architecture of the three TBC systems prepared for the current study is also shown schematically in Fig. 2.

3. Finite element modeling

3.1. Description of the model

A finite element (FE) model was developed to evaluate the distribution of residual stresses within the coated specimens using ANSYS 14.5 (APDL). The model geometry used in the analysis represents a disc shaped Nimonic 90 substrate of 12.8 mm in diameter and 3.0 mm in thickness with layers of coatings deposited on the surface of the substrate as shown in Fig. 3. The types and thickness of the coatings considered in the present study are summarized in Table 3. Three coating systems considered in this study were prepared with the same overall thickness of 300 μm but variation in individual layers thicknesses (Table 3). A coupled thermal-structural finite element analysis was employed using 2-D coupled field element PLANE223 having eight nodes with up to maximum four degrees of freedom per node. Mapped grid was used for meshing the model due to solid entities thereby generating regular and computationally well behaving mesh.

An axisymmetric model was chosen in order to reduce the data processing time as shown in Fig. 3(b). All the interfaces were assumed to be flat and the effect of grit blasting prior to deposition process was neglected. It was assumed that bonding between the deposited layers was perfect and the effect of porosity was ignored. Moreover, the bonding between the coating and the substrate was also considered defect free. The substrate and the coatings were considered to be homogeneous and isotropic for simplicity. The boundary conditions related to heat transfer used in the analysis are shown in Fig. 4. The model was subjected to a thermal load of 400 °C on the top surface of the coating and the bottom of the substrate was maintained at 20 °C. The displacement in X-direction (radial direction) was constrained along the line of symmetry for the structural analysis. The entire specimen was assumed to be stress free at the reference temperature of 400 °C at which the spraying process was supposed to end. The final residual stresses were assumed to be generated only due to the cooling of the whole coating system from the reference temperature of 400 °C to 20 °C. Heat convection was imposed on the top surface and side of the specimen as shown in Fig. 4. A heat transfer coefficient (h) of 25 W/m^2 °C was used. Steady-state analysis was performed to analyze the residual stress distribution within the coating systems.

Residual stress components resulting from the FEA were obtained in the following directions: (1) radial stresses corresponding to stress value along the radial direction, (2) axial stress component referring to stress profile through thickness of coatings and (3) shear stress component acting along the tangential direction.

3.2. Temperature and composition-dependent material properties

It is well known that the thermo-physical properties of Ni and MSZ vary with temperature and the properties of their

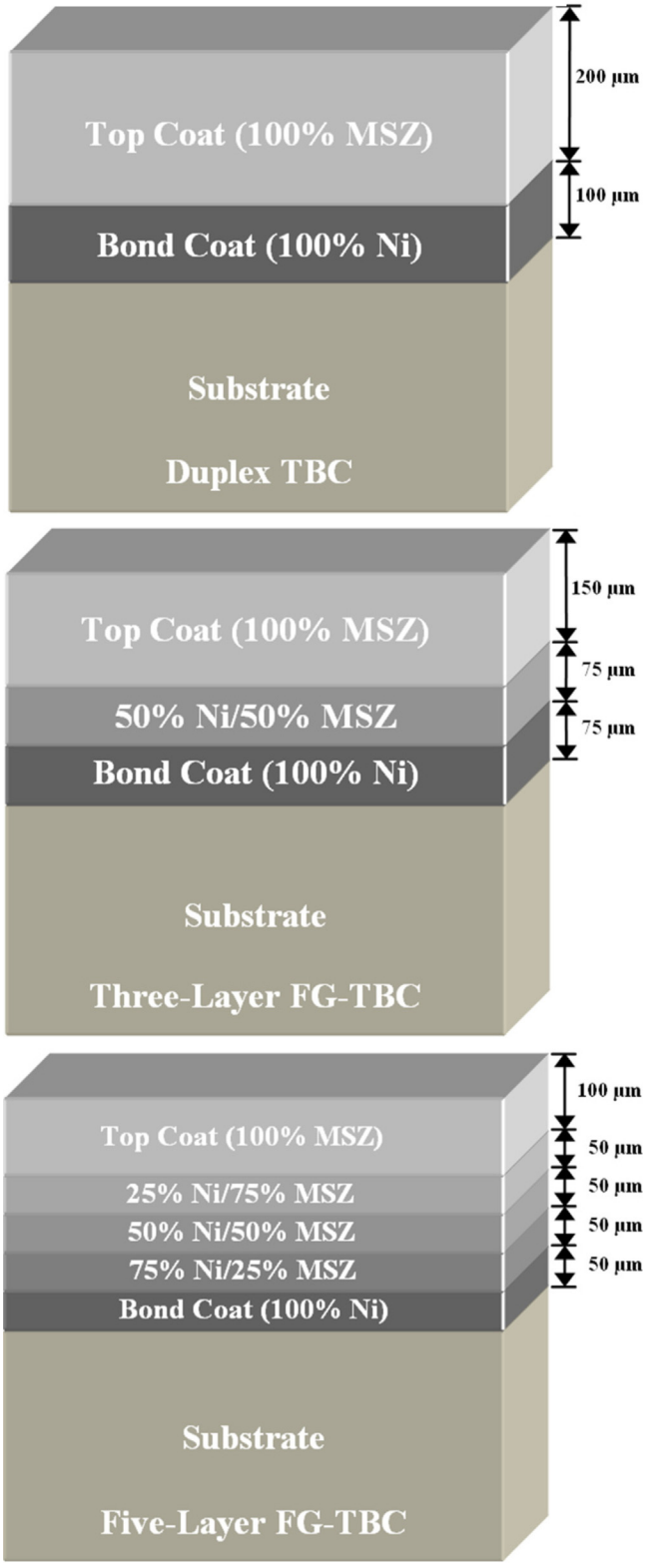

Fig. 2. Schematic diagrams showing architecture of the three TBC systems.

mixtures depend strongly on the composition of the mixture. Previous researchers have either used temperature-dependent or composition-dependent material properties of the mixtures for their FE analysis, but the temperature and compositional effects onto the material properties of the TBCs were not

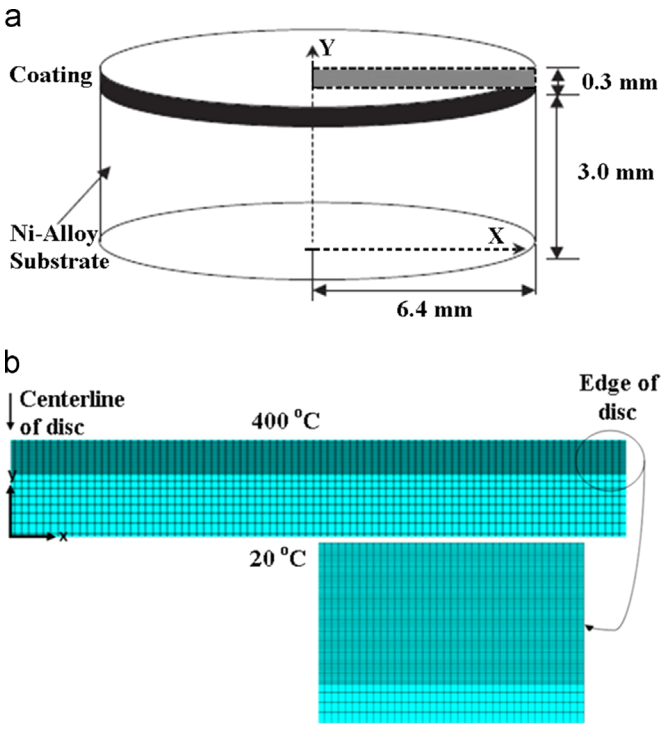

Fig. 3. Schematic description of the geometry (a) and FE details of the axisymmetric model (b) used for analysis.

incorporated together and applied concomitantly. In the current investigation, both the temperature and the composition-dependent material properties were used for FE analysis in order to achieve a more practical simulation. The temperature-dependent properties of Ni and MSZ were taken from literature [15,36–39] and the composition-dependent properties against each temperature were calculated using the Vegard's rule [35]

$$M_i = M_A(V_A)_i + M_B * (1-(V_A)_i)$$

where M_i is the material property of the ith layer, M_A is the material property of material A, $(V_A)_i$ is the volume fraction of component A in the ith layer, M_B is the material property of material B. The temperature and composition-dependent material properties of all the layers used in the present study are given in Table 4.

4. Results and discussion

4.1. Characterization of coatings

SEM micrographs of polished cross sections of the three TBC systems, a duplex and two functionally graded (three and five-layer FG-TBCs), are shown in Fig. 5. The duplex TBC system as shown in Fig. 5(a), shows a visible boundary between the two deposited layers and the dense Ni layer can be clearly distinguished from the porous MSZ layer. However, no sharp boundaries were formed between the layers in case of functionally graded coatings and their structure was observed to be relatively continuous as compared to duplex TBC system. The gradient distribution of the two phases in the functionally graded coatings can appreciably reduce the high

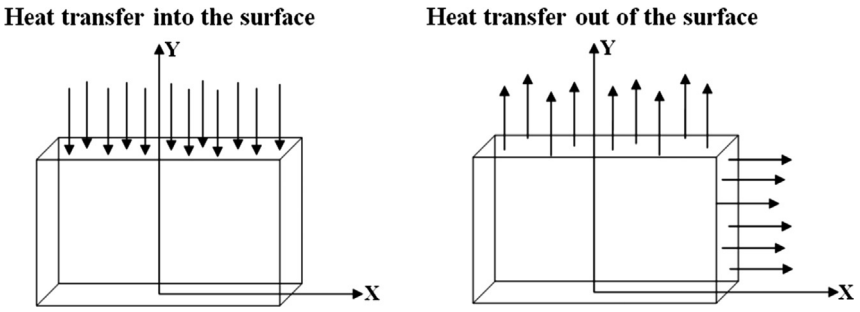

Fig. 4. Schematic diagram showing heat transfer boundary conditions used in FEA.

Table 4
Temperature and composition-dependent material properties used in FE analysis.

Material	Temperature (°C)	Density (Kg/m^3)	Elastic modulus (GPa)	Poison's ratio	CTE (10^{-6}/°C)	Thermal conductivity (W/m °C)	Specific heat (J/Kg °C)
Nimonic 90	20	8180	204	0.28	12.7	11.47	446
	100	8180	199	0.28	13.3	12.77	467
	200	8180	194	0.28	13.7	14.44	494
	300	8180	188	0.28	14.0	15.99	520
	400	8180	181	0.28	14.3	17.54	547
Ni	20	7200	83	0.29	8.972	11.5	500
	100	7200	83	0.29	11.710	13.0	512.9
	200	7200	83	0.29	12.910	14.7	521.3
	300	7200	83	0.29	13.670	15.9	529.6
	400	7200	83	0.29	14.170	16.7	543.9
75 Ni/25 MSZ	20	6457	77	0.286	7.661	7.954	523.8
	100	6457	77	0.286	10.246	8.953	545.9
	200	6457	77	0.286	11.512	10.089	564.3
	300	6457	77	0.286	12.368	10.852	580.6
	400	6457	77	0.286	12.880	11.376	600.3
50 Ni/50 MSZ	20	5872	72	0.259	6.629	5.163	542.5
	100	5872	72	0.259	9.094	5.767	571.8
	200	5872	72	0.259	10.412	6.459	598.2
	300	5872	72	0.259	11.343	6.879	620.8
	400	5872	72	0.259	11.865	7.185	644.7
25 Ni/75 MSZ	20	5400	68	0.249	5.796	2.911	557.6
	100	5400	68	0.249	8.164	3.196	592.7
	200	5400	68	0.249	9.524	3.530	625.5
	300	5400	68	0.249	10.516	3.672	653.3
	400	5400	68	0.249	11.046	3.803	680.5
MSZ	20	5010	65	0.24	5.109	1.053	570
	100	5010	65	0.24	7.397	1.076	610
	200	5010	65	0.24	8.792	1.115	648
	300	5010	65	0.24	9.834	1.028	680
	400	5010	65	0.24	10.370	1.014	710

thermal stresses generated due to the sharp differences in CTE and elastic modulus between the two phases for duplex coating. The presence of such high thermal and mechanical stresses generated at the interface of the two layers during the thermal and mechanical loading may cause bond strength to reduce and therefore the coating is likely to crack or spall [29].

Vickers microhardness (HV0.3) of the five individual coatings was measured and drawn in three different combinations

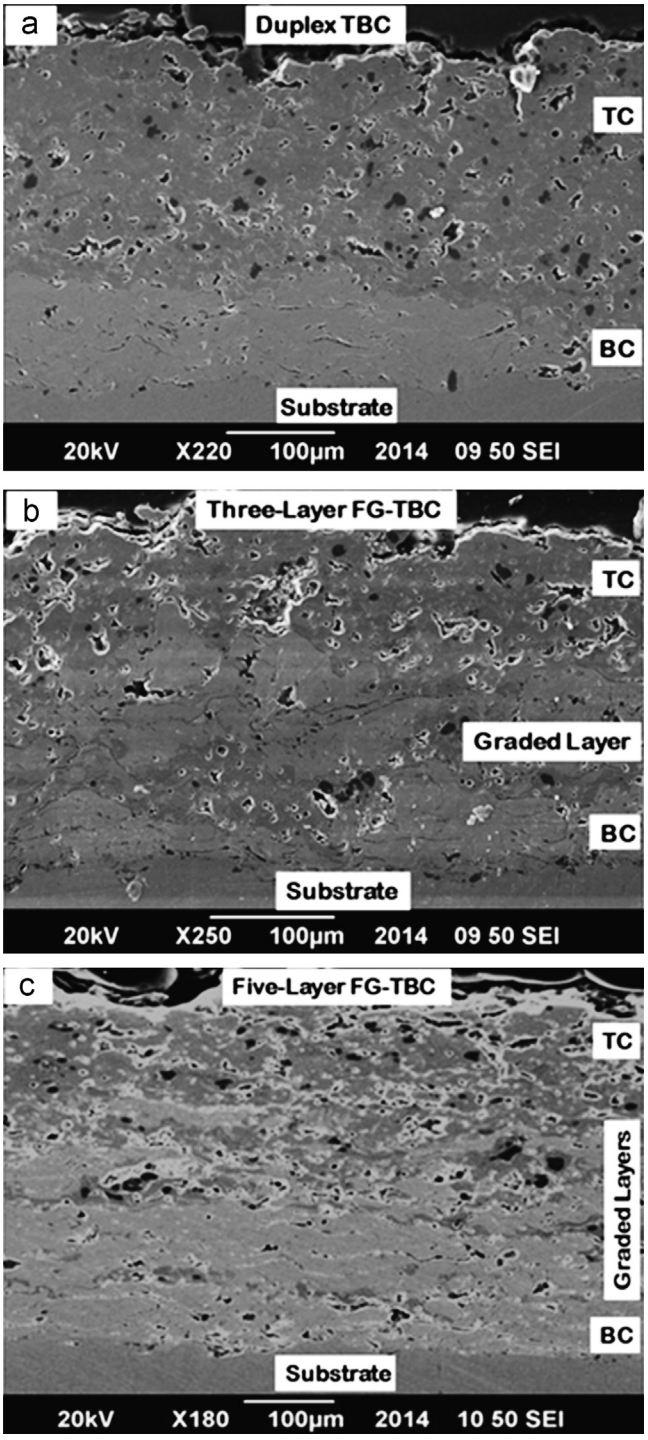

Fig. 5. SEM micrographs showing microstructure of the coating in, (a) duplex, (b) three-layer FG-TBC and (c) five-layer FG-TBC.

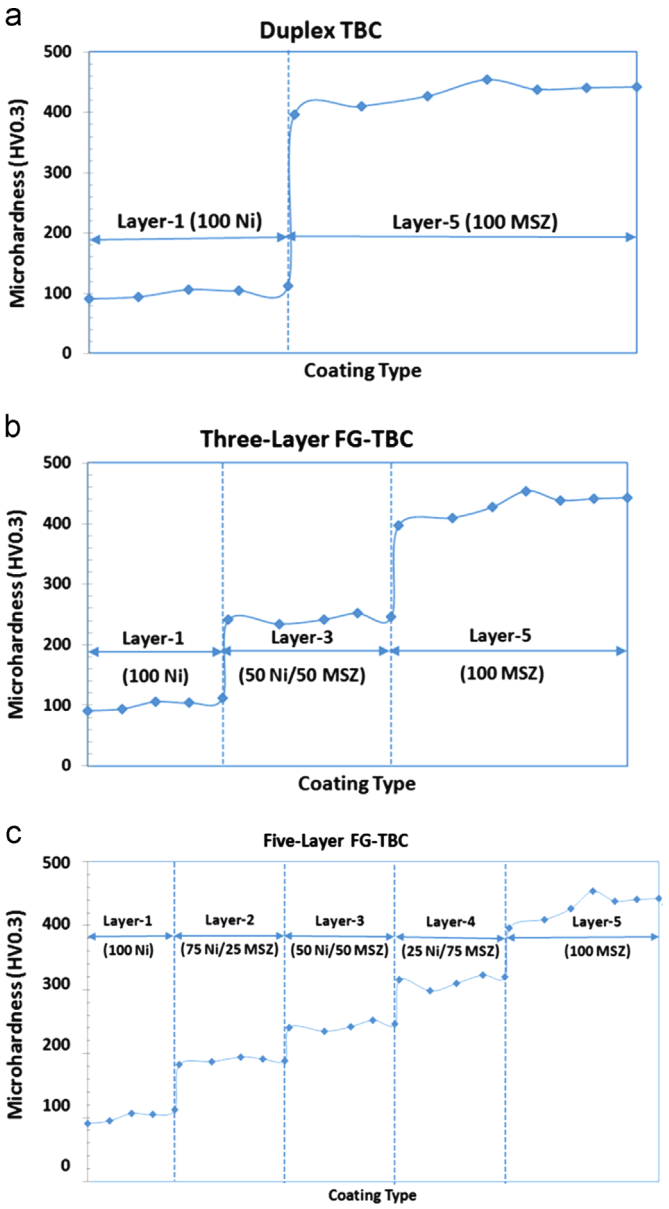

Fig. 6. Microhardness distributions of the three TBC systems, (a) duplex, (b) three-layer FG-TBC and (c) five-layer FG-TBC.

to simulate the three coating systems as shown in Fig. 6. In the duplex coating system as shown in Fig. 6(a), there was a large difference between the microhardness values of the two layers, i.e., varying from approximately 112 (HV0.3) in the BC to 396 (HV0.3) in the TC. This steep difference in microhardness, as shown in Fig. 6(b), was somewhat divided into two smaller portions in case of three-layer FG-TBC system, i.e., from approximately 112 (HV0.3) to 241 (HV0.3) at the BC/intermediate layer (50 Ni/50 MSZ) interface and from 245 (HV0.3) to 396 (HV0.3) at the intermediate layer/TC interface, thus avoiding a large difference in microhardness values as compared to the duplex system. This reduction in difference of microhardness values between the two TBC systems might be expected to reduce the magnitude of the residual stresses in the three-layer FG-TBC system as compared to duplex TBC due to a reduced mismatch in the properties at the two interfaces of the three-layer FG-TBC system [29].

In the case of five-layer FG-TBC system as shown in Fig. 6(c), it can be observed that the microhardness changed gradually through the five layers as compared to other two TBC systems in such a way that a sharp mismatch could be avoided. Therefore, it is expected that the absence of a sharp mismatch in microhardness due to the presence of compositionally gradient layers may cause suppression in the development of otherwise high residual

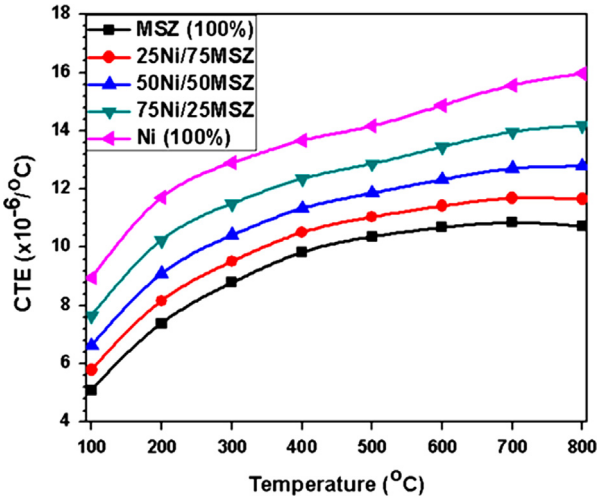

Fig. 7. CTE plot as a function of temperature for five individual layers.

stresses at the interfaces thus increasing the expected life of the five-layer FG-TBC system [29,34–35].

Fig. 7 shows the linear CTE of the five individual layers as a function of temperature from room temperature to 800 °C. It can be observed from Fig. 7 that CTE of the five individual layers increased with an increase in temperature and gradually changed through the five layers. A considerable difference between the CTE values of the two deposited layers comprising the duplex TBC system, namely Ni and MSZ was observed which further increased as the temperature is increased. Therefore, large thermal and mechanical stresses are expected to be generated at the interface of the two layers during thermal and mechanical loading owing to the large mismatch in CTE resulting in a premature failure of the duplex TBC system [29].

In the case of three-layer FG-TBC system which was prepared by incorporating an intermediate layer of 50 Ni/50 MSZ powder mixture between the BC and TC, this difference in CTE decreased to some extent but there was still a sizeable gap between the CTE of the three deposited layers. This system might be expected to possess a lower level of thermal and mechanical stresses because of its lower CTE mismatch between the three deposited layers and consequently expected to perform better under same thermal and mechanical loads than the duplex TBC system [29].

For five-layer FG-TBC system, there was a gradual increase in the CTE values of the five coated layers thereby steadily reducing the difference between their CTE. This gradual variation in CTE between the five deposited layers may be expected to further reduce the level of thermal and mechanical stresses within the five-layer FG-TBC system as compared to duplex and three-layer TBC systems. It may therefore be expected that five-layer FG-TBC may exhibit better thermal shock resistance and hence improved cyclic life under similar thermal and mechanical loads as compared to other two TBC systems.

4.2. Residual stress distribution for duplex and FG-TBCs

Fig. 8(a)–(c) shows the typical contour plots of radial stress distribution in the three coating systems, one duplex and two FG-TBCs (three and five-layered). It was observed that compressive stresses were generated in the surface in all the three coating systems which gradually changed to tensile with an increase in the distance from the surface into the coating. The maximum radial stress observed in all the three coating systems was below the MSZ layer, i.e., at the interface of the TC and the adjacent layer below it. A remarkable stress concentration was seen at the center of the specimen for all three coating systems decreasing near the edge and the incorporation of intermediate layer/s only changed the level of the stress and did not change the pattern of stress distribution. The maximum compressive and tensile radial stresses generated in the three TBC systems decreased with an increase in number of layers from duplex to five-layer FG-TBC.

Typical contour plots of axial stress distribution in the three coating systems are shown in Fig. 9(a)–(c). The maximum compressive and tensile axial stresses in all the three coating systems were observed near the edge of the specimen at the top cot/underneath layer interface and substrate/BC interface, respectively. The tensile stress was observed near the edge of the specimen which decreased abruptly and changed to compressive stress with the increase of specimen radius. The concentration of large residual stress near the edge of the specimen and the presence of large tensile and compressive axial stresses at the edge may result in microcracks normal to the interface and buckling and spallation of the coating, respectively. By incorporating the functionally gradient interlayers between the bond and top coats, the maximum compressive axial stresses decreased significantly but the maximum tensile axial stresses increased considerably.

Typical contour plots of shear stress distribution in the three coating systems are presented in Fig.10(a)–(c). The maximum shear stress in all the three coating systems was found to be compressive and concentrated near the edge of the specimen mainly above the BC, i.e., at the interface of BC and the adjacent layer above it. The value of compressive and tensile shear stresses decreased with an increase in number of layers from duplex to five-layer FG-TBC but this difference was not as large as in case of radial and axial stresses.

The decrease in residual stresses by incorporating the functionally gradient interlayers may be due to the reduced CTE mismatch between the layers which led to lower thermal gradients and lower level of residual stresses in the FG-TBC systems [29,40–41].

4.3. Residual stress distribution for five-layer FG-TBC

Fig. 11(a)–(c) shows the residual stress distributions on the surface and interfaces of the five-layer FG-TBC plotted along the radius of the coating after cooling from the spraying temperature of 400 °C to 20 °C. It was observed (Fig. 11(a)) that radial stress at the surface of the coating was usually compressive which gradually changed to tensile along the thickness of the coating. At the surface and substrate/BC interface, the radial stress was compressive and an abrupt increase was observed in this compressive stress near the edge of the specimen. The coating surface was found in a state of compression and a maximum compressive radial stress of

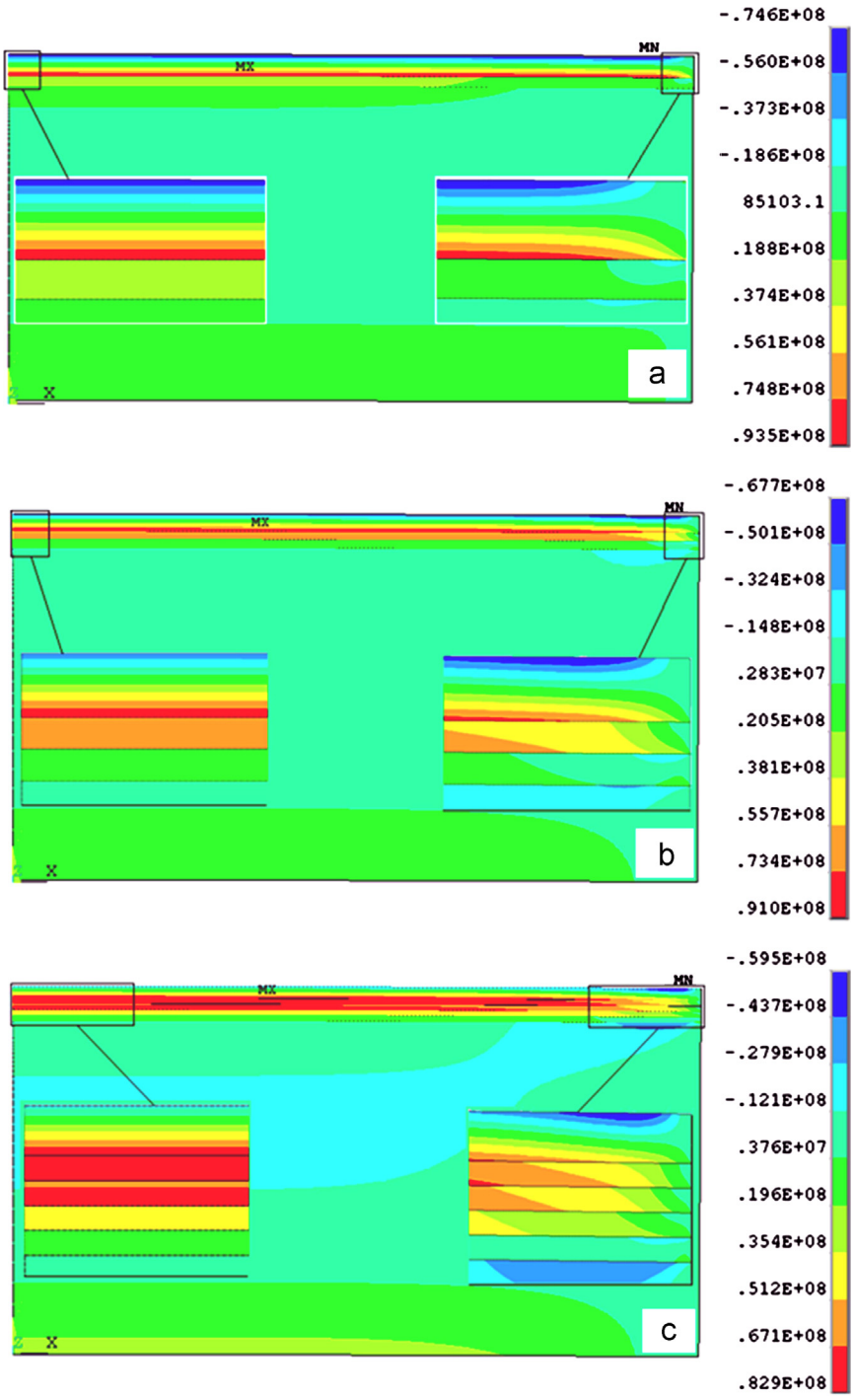

Fig. 8. Typical contour plots of radial stress distribution of the three coating systems, (a) duplex, (b) three-layer FG-TBC and (c) five-layer FG-TBC.

approximately 60 MPa was identified at the surface of the coating near the edge. The BC, however, was found slightly in a state of tension near the center along the radial direction but became compressive approaching the edge and a maximum compressive stress of about 23 MPa was identified near the edge. A minor variation in behavior of BC from compressive to tensile was observed near the edge and a tensile radial stress of about 6 MPa was identified at the edge. At other interfaces of the coating, i.e., 100 Ni (BC)/75 Ni, 75 Ni/50 Ni, 50 Ni/25 Ni and 25 Ni/0 Ni (TC), the stresses were found to be tensile and the maximum tensile stress of approximately 76 MPa was observed at 25 Ni/0 Ni (TC) interface near the center of the specimen abruptly decreasing to zero near the edge.

The distribution of axial stress at the interfaces of the five-layer FG-TBC is shown in Fig. 11(b). It was observed that the axial stresses generated at the substrate/BC and BC/75 Ni interfaces were tensile in nature and a maximum of about 71 MPa of tensile axial stress was generated at the edge. The axial residual stresses generated at other interfaces of the coating, i.e., 75 Ni/50 Ni, 50 Ni/25 Ni and 25 Ni/0 Ni (TC),

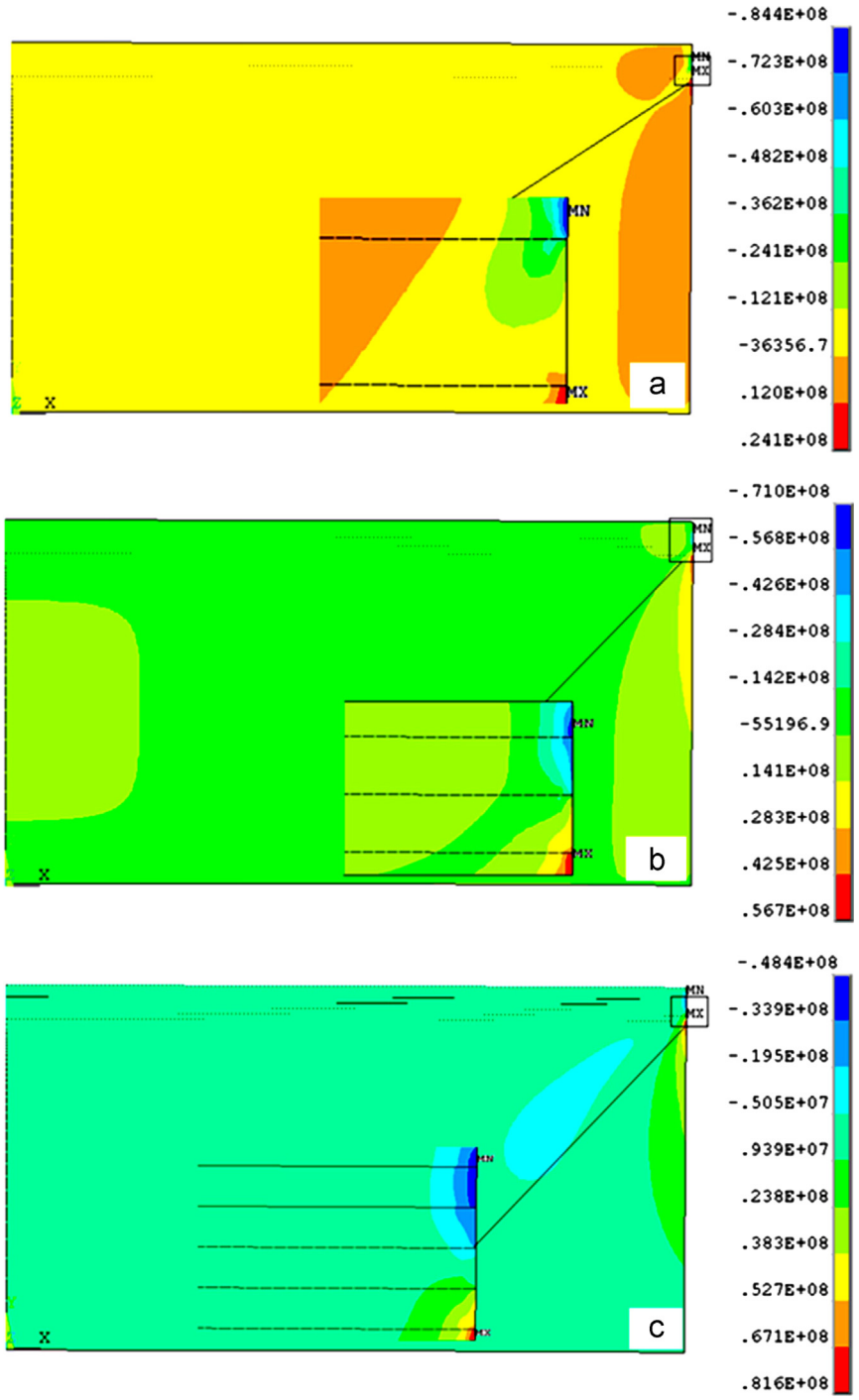

Fig. 9. Typical contour plots of axial stress distribution of the three coating systems, (a) duplex, (b) three-layer FG-TBC and (c) five-layer FG-TBC.

were found to be compressive in nature and a maximum of about 48 MPa compressive axial stress was found to be generated at the 25 Ni/0 Ni (TC) interface at the edge. Near the edge of these interfaces, the axial stress first became slightly tensile and then abruptly changed to compressive with a maximum value at the edge of the specimen. The axial stresses were found to be decreased quickly with an increase in the distance from the edge of the specimen.

Fig. 11(c) shows the distribution of shear stress along the radius for a five-layer FG-TBC. The shear stresses at all the interfaces were found to be mainly compressive in nature with a maximum value of about 23 MPa at the BC/75 Ni interface near the edge.

It is well documented in literature that, from the residual stress distribution standpoint, surfaces and interfaces between dissimilar materials are the locations of interest because of the mismatch in their properties such as elastic modulus and CTE [40]. It has also been documented that the modes of failure in coatings strongly depend on the tensile or compressive nature of the residual stresses [41]. Tensile residual stresses may

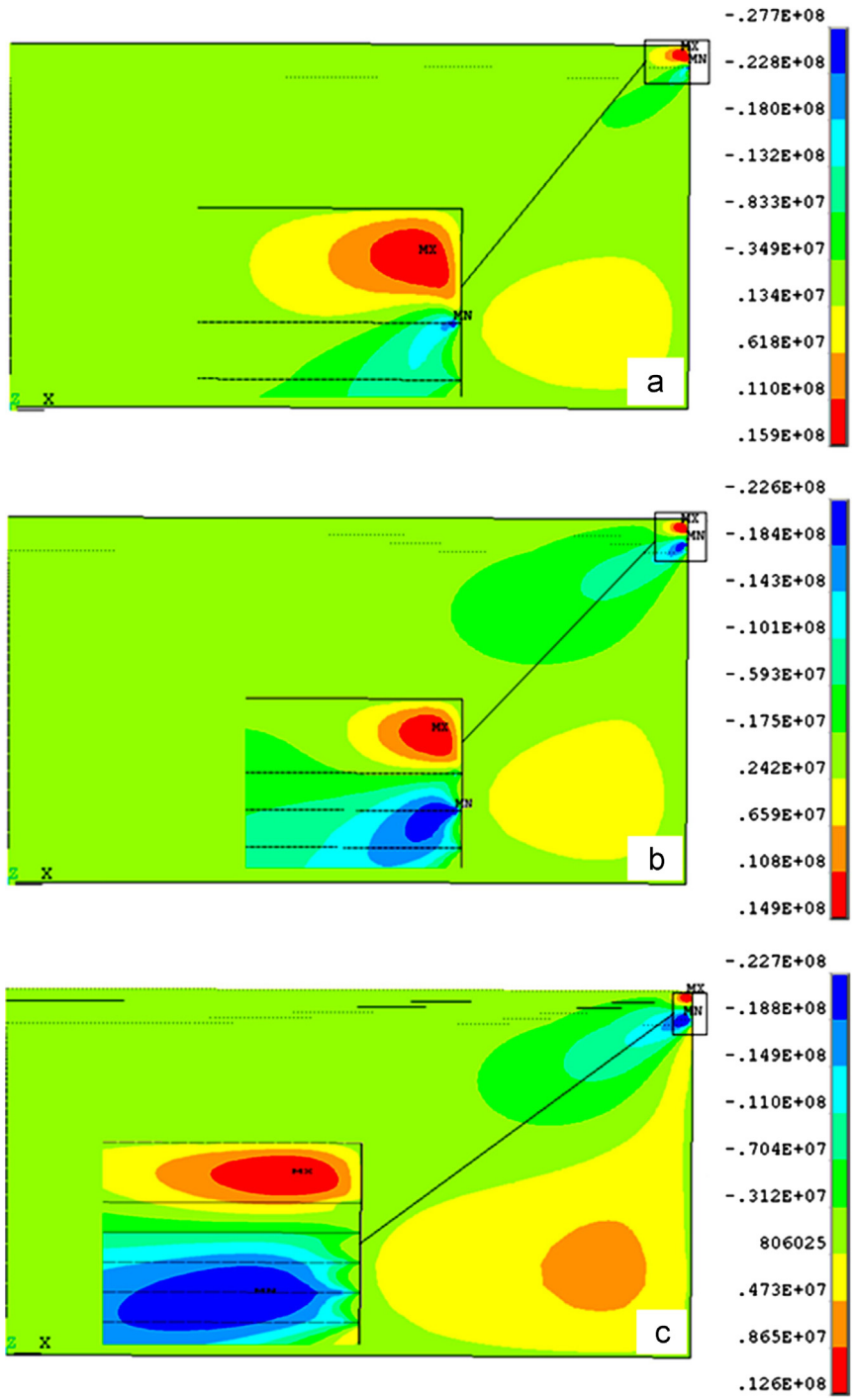

Fig. 10. Typical contour plots of shear stress distribution of the three coating systems, (a) duplex, (b) three-layer FG-TBC and (c) five-layer FG-TBC.

induce fracture of the coating normal to the interface by producing microcracks perpendicular to the interface whereas compressive residual stresses can originate buckling and ultimate spallation of the coating. It has been demonstrated that compressive residual stresses can initiate and propagate interfacial cracks which may or may not result in the spallation of the coating depending on the relative fracture strengths of the interface and coating [40–41]. It can be concluded from the above discussion that generation of large compressive radial stresses at the surface may cause buckling of the coating whereas large tensile radial stresses generated at the interfaces may result in crack initiation and propagation perpendicular to the coating interface. Similarly, the presence of large axial and shear stresses at the interfaces and their concentration near the edge of the specimen may cause spallation of the coating.

4.4. Effect of coating layers on residual stresses

Fig. 12(a)–(c) shows the maximum radial, axial and shear stresses in the duplex and three and five-layer FG-TBCs having

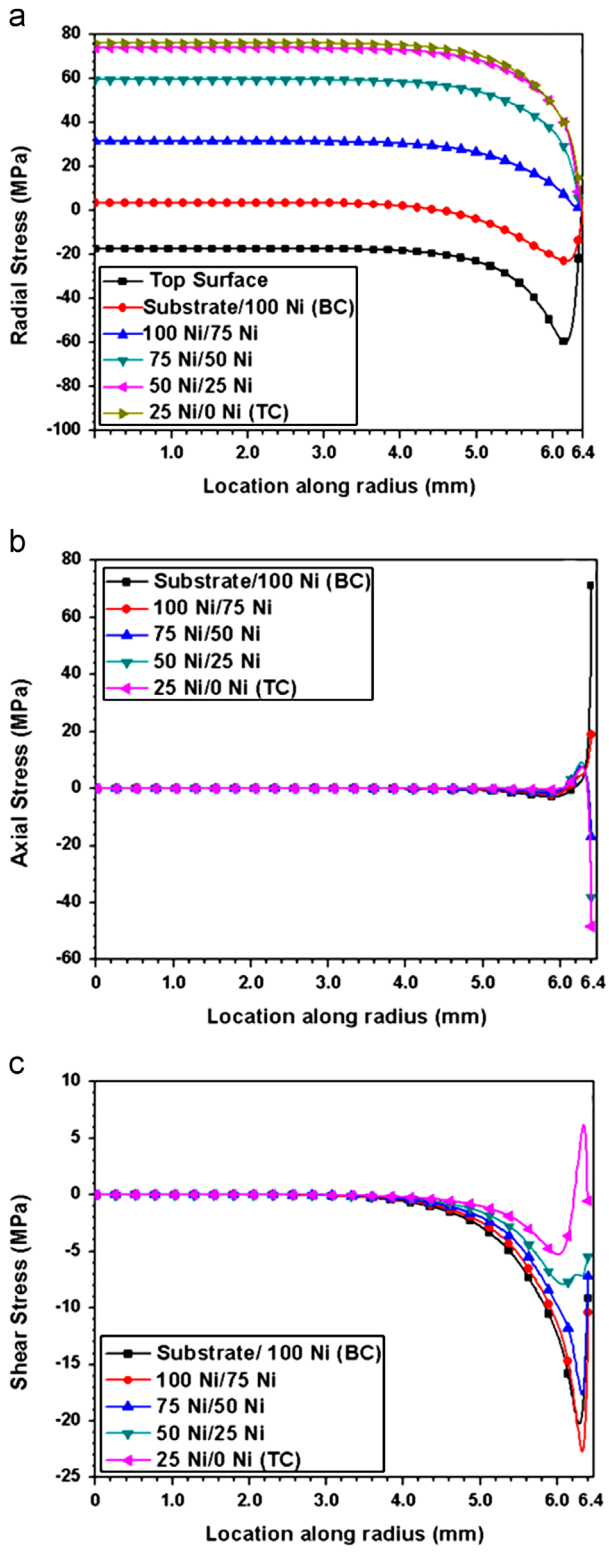

Fig. 11. Residual stress distribution along the radius of coating for five-layer FG-TBC, (a) radial stress, (b) axial stress and (c) shear stress.

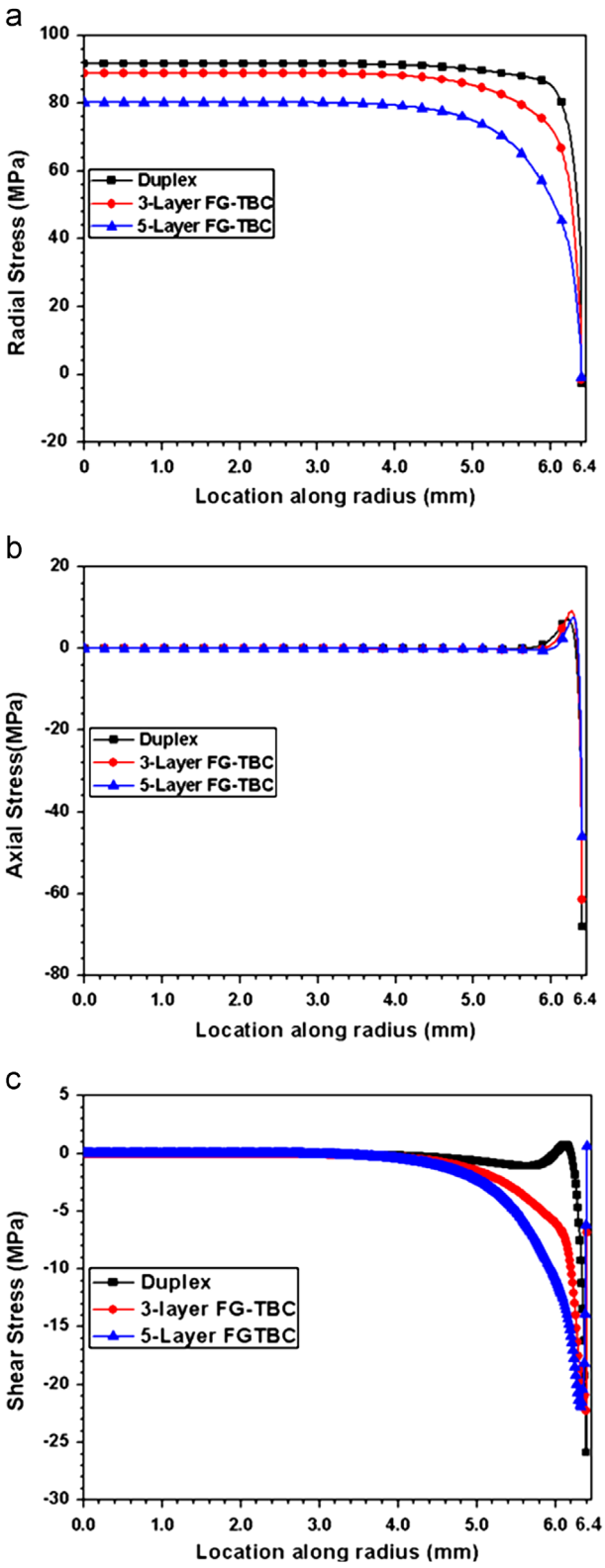

Fig. 12. Comparison of stresses in the three TBC systems having different number of layers but with same thickness, (a) radial stress, (b) axial stress and (c) shear stress.

equal overall thickness but with different number of layers. It can be observed from Fig. 12 that the highest residual stresses were generated within the duplex TBC, whereas minimum residual stresses were produced within the five-layer FG-TBC. The incorporation of functionally gradient layer/s between the bond and top coats can have a significant effect on the level of residual stresses generated within the FG-TBC systems [29,40–41]. The residual stresses formed within the three-layer FG-TBC after

plasma spraying were relaxed by incorporating an intermediate layer consisting of 50 Ni/50 MSZ between the BC and TC. This intermediate layer resulted in a reduced CTE mismatch between the deposited layers as compared with duplex TBC thus resulting in less residual stresses within the system. However, when comparing the two FG-TBC systems, it was observed that the residual stresses generated within the five-layer FG-TBC were comparatively lower. This reduction in residual stresses within the five-layer FG-TBC can be attributed to the gradual change in the CTE of the five deposited layers owing to the composition of each individual layer as described in Table 4. It was found that the maximum radial stress for five-layer FG-TBC, compared with that of duplex coating, decreased by 15.5 MPa, whereas maximum compressive axial stress and shear stress reduced by 22.3 and 4.0 MPa, respectively. The maximum redial stress and maximum axial stress in all the three TBC systems were found to be below the MSZ layer and the maximum shear stress was above the BC.

It can be concluded from the above analysis that the five-layer FG-TBC exhibited lowest radial, axial and shear stresses compared with those of the duplex and three-layer FG-TBC. This reduced level of residual stresses in the five-layer FG-TBC might result in an increased bond strength and better thermal cycle resistance as compared with duplex and three-layer FG-TBC under same thermal and mechanical loading conditions and expected to increase the life of the FG-TBCs [29].

4.5. Bond strength

Bond strength is an important factor determining the life of the thermally sprayed coatings. Average bond strengths (adhesion/cohesion strengths) of the three TBC systems were measured as per ASTM standard C633-01 and are shown in Fig. 13. Both the FG-TBC systems were found to have higher bond strengths than the duplex TBC, however, five-layer FG-TBC showed the highest bond strength amongst these three systems.

In case of FG-TBCs, the composition of layers gradually changed from purely metallic (BC) to metallic/ceramic mixtures (intermediate cermet layer/s) to purely ceramic (TC). This gradual compositional variation between the layers resulted in reduced levels of residual stresses which otherwise might be quite high in case of duplex TBC due to compositional mismatch at the interface. Additionally, barely visible interfaces were found between the adjacent layers in FG-TBCs thus resulting in an almost continuous microstructure as compared to duplex coating which possessed a sharp boundary and a discontinuous microstructure between the BC and TC. Furthermore, the fracture toughness of the BC might be much higher due to its metallic nature as compared to the ceramic TC. Consequently, the presence of metallic Ni in the functionally graded layer/s might improve overall fracture toughness of the coating system and the crack growth rate maybe decreased [27]. All these factors are believed to be the major contributors in improving the bond strengths of the FG-TBCs [27,31–32,42].

The variation in bond strengths of the three TBC systems can be explained from FEA results shown in Fig. 12 by correlating the level of residual stresses generated and their concentration location in different TBC systems. In case of duplex TBC, the radial, axial and shear stresses were extremely high as can be seen from Fig. 12. The presence of such high level of residual stresses may cause the duplex coating system to crack, spall and delaminate. This was the reason why duplex TBC showed minimum bond strength as compared to FG-TBCs. The level of these residual stresses can be reduced appreciably by incorporating functionally gradient interlayers between the BC and TC as can be seen in Fig. 12. It can be observed that the residual stresses generated in five-layer FG-TBC were comparatively lower than three-layer FG-TBC explaining the relatively high bond strength of the former.

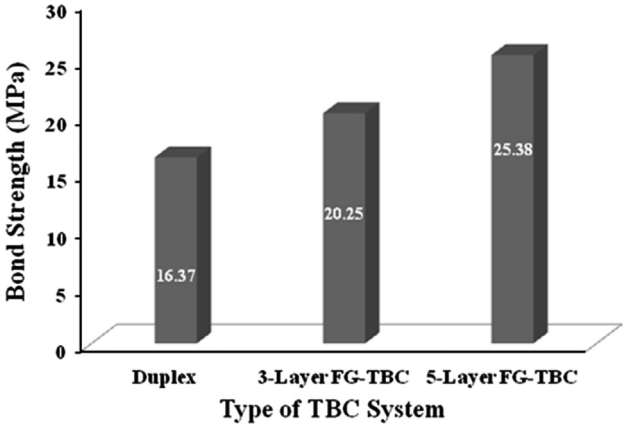

Fig. 13. Average bond strengths of the three TBC systems.

Fig. 14 shows photographs of the fractured samples of three TBC systems. In duplex and three-layer FG-TBC, the fractures were found to be of internal adhesive/adhesive nature, i.e., they fractured at ceramic-BC and ceramic-intermediate cermet layer interface, respectively, as shown in Fig. 14(a) and (b). In case of five-layer FG-TBC, however, a complex cohesive/adhesive mode of fracture was observed. The cohesive fracture was seen at the epoxy-ceramic interface whereas adhesive fracture was observed within the cermet layers and at the substrate-BC interface as shown in Fig. 14(c). The fracture loci of all the three TBCs were found to be in compliance with the FEA results shown in Fig. 8–Fig. 10 in the form of contour plots.

5. Conclusions

Three multilayered coating systems were prepared to examine the stability and stress distribution using experimental and modeling techniques. The microstructure, microhardness and coefficient of thermal expansion were found to gradually change in the five-layer FG-TBC as compared with duplex and three-layer FG-TBC.

The finite element analysis showed development of compressive radial stresses that were observed near the surface in all the three coating systems which may result in microcracking of coating layers. The maximum radial stress observed in all the three coating systems was below the MSZ layer whereas the maximum axial and shear stresses were found near the edge which may lead to coating failure or spallation.

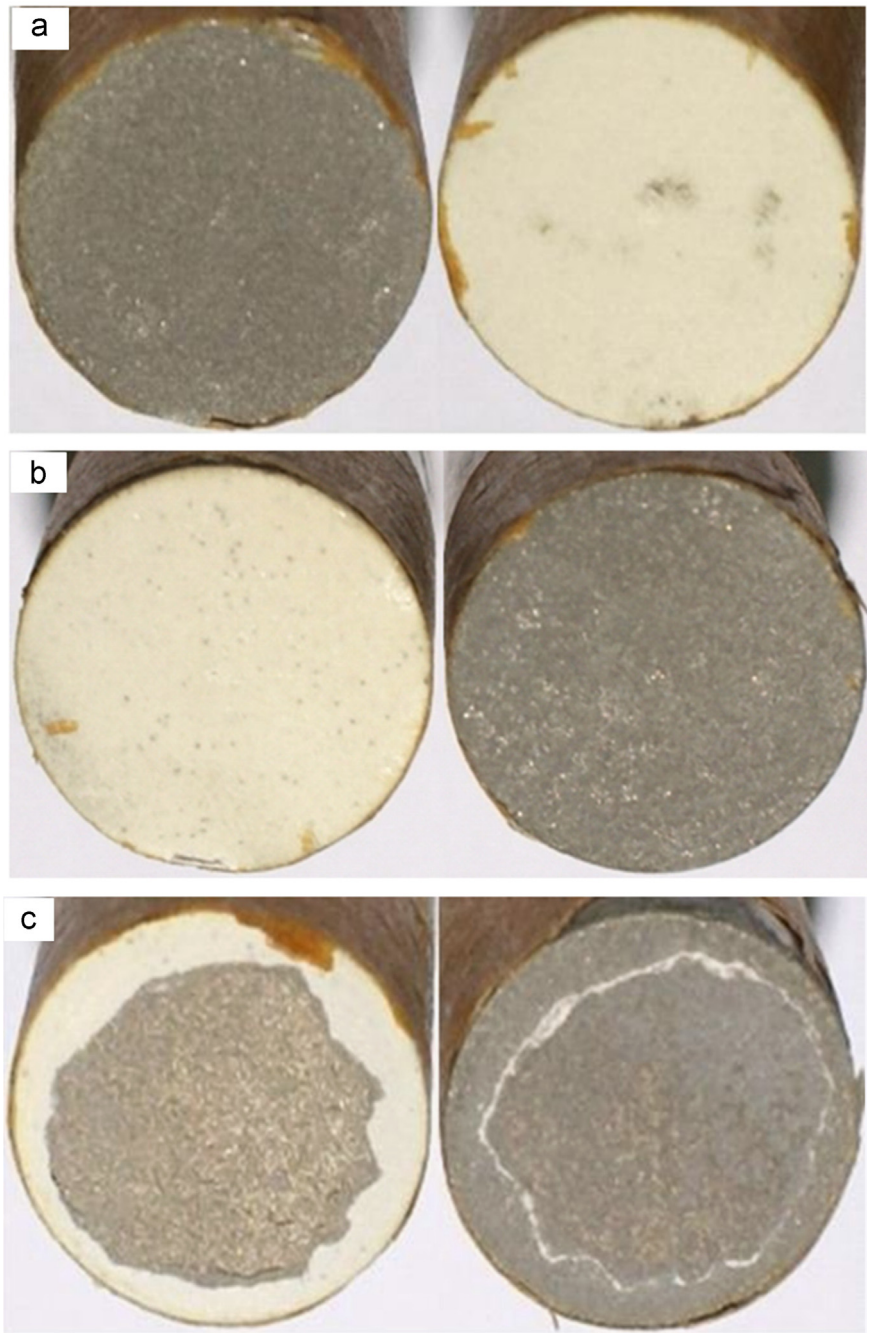

Fig. 14. Fractured surfaces of the three coating systems showing location of failure (failure locus), (a) duplex, (b) three-layer FG-TBC and (c) five-layer FG-TBC.

It was found that five-layer FG-TBC had the lowest radial, axial and shear stresses compared with those of the duplex and three-layer FG-TBC. The reduction in residual stresses in the five-layer FG-TBC is probably due to decrease in mismatch of the CTE of the deposited layers.

Increasing the number of layers with a gradient in composition from bond coat to top coat with similar coating thickness ultimately increased the bond strength of the FG-TBCs. The bond strength of five-layer FG-TBC was found to be almost 1.5 times higher than that of the duplex TBC.

It can be concluded that the five-layer FG-TBC design can be beneficial to prevent generation of thermal stresses as compared to the duplex TBC.

Acknowledgments

M. N. Baig would like to thank the Higher Education Commission of Pakistan (HEC) for providing financial assistance and PIEAS, PINSTECH & NUST for use of facilities.

References

[1] Y.Y. Zhang, H.X. Deng, H.J. Shi, H.C. Yu, B. Zhong, Failure characteristics and life prediction for thermally cycled thermal barrier coatings, Surface and Coatings Technology 206 (2012) 2977–2985.

[2] M. Okazaki, S. Yamagishi, Y. Yamazaki, K. Ogawa, H. Waki, M. Arai, Adhesion strength of ceramic top coat in thermal barrier coatings subjected to thermal cycles: effects of thermal cycle testing method and environment, International Journal of Fatigue 53 (2013) 33–39.

[3] X. Wang, S. Tint, M. Chiu, A. Atkinson, Stiffness of free-standing thermal barrier coating top coats measured by bending tests, Acta Materialia 60 (2012) 3247–3258.

[4] C. Bargraser, P. Mohan, K. Lee, B. Yang, J. Suk, S. Choe, Y.H. Sohn, Life approximation of thermal barrier coatings via quantitative microstructural analysis, Materials Science and Engineering: A 549 (2012) 76–81.

[5] C.S. Ramachandran, V. Balasubramanian, P.V. Ananthapadmanabhan, V. Viswabaskaran, Influence of the intermixed interfacial layers on the thermal cycling behaviour of atmospheric plasma sprayed lanthanum zirconate based coatings, Ceramics International 38 (2012) 4081–4096.

[6] S. Yugeswaran, A. Kobayashi, P.V. Ananthapadmanabhan, Hot corrosion behaviors of gas tunnel type plasma sprayed $La_2Zr_2O_7$ thermal barrier coatings, Journal of the European Ceramic Society 32 (2012) 823–834.

[7] S. Kumar, A.C.F. Cocks, Sintering and mud cracking in EB-PVD thermal barrier coatings, Journal of the Mechanics and Physics of Solids 60 (2012) 723–749.

[8] M. Billah Bhatty, F. Ahmad Khalid, A. Nusair Khan, Behavior of calcia-stabilized zirconia coating at high temperature, deposited by air plasma spraying system, Journal of Thermal Spray Technology 21 (2012) 121–131.

[9] J.J. Liang, K. Matsumoto, K. Kawagishi, H. Harada, Morphological evolution of thermal barrier coatings with equilibrium (EQ) and NiCoCrAlY bond coats during thermal cycling, Surface and Coatings Technology 207 (2012) 413–420.

[10] C.U. Hardwicke, Y.-C. Lau, Advances in thermal spray coatings for gas turbines and energy generation: a review, Journal of Thermal Spray Technology 22 (5) (2013) 564–576.

[11] S.-H. Song, P. Xiao, L.-Q. Weng, Evaluation of microstructural evolution in thermal barrier coatings during thermal cycling using impedance spectroscopy, Journal of the European Ceramic Society 25 (2005) 1167–1173.

[12] C. Pan, X. Xu, Microstructural characteristics in plasma sprayed functionally graded ZrO_2/NiCrAl coatings, Surface and Coatings Technology 162 (2003) 194–201.

[13] S. Darzens, A.M. Karlsson, On the microstructural development in platinum-modified nickel–aluminide bond coats, Surface and Coatings Technology 177/178 (2004) 108–112.

[14] K.A. Khor, C.T. Chia, Y.W. Gu, Dynamic mechanical properties of plasma sprayed Ni-based alloys, Materials Science and Engineering: A 279 (2000) 166–171.

[15] S. Sampath, X.Y. Jiang, J. Matejicek, L. Prchlik, A. Kulkarni, A. Vaidya, Role of thermal spray processing method on the microstructure, residual stress and properties of coatings: an integrated study for Ni–5 wt%Al bond coats, Materials Science and Engineering: A 364 (2004) 216–231.

[16] R.A. Mahesh, R. Jayaganthan, S. Prakash, Oxidation behavior of HVOF sprayed Ni–5Al coatings deposited on Ni- and Fe-based superalloys under cyclic condition, Materials Science and Engineering: A 475 (2008) 327–335.

[17] M. Shinozaki, T.W. Clyne, The effect of vermiculite on the degradation and spallation of plasma sprayed thermal barrier coatings, Surface and Coatings Technology 216 (2013) 172–177.

[18] H. Choi, B. Yoon, H. Kim, C. Lee, Isothermal oxidation of air plasma spray NiCrAlY bond coatings, Surface and Coatings Technology 150 (2002) 297–308.

[19] A. Portinha, V. Teixeira, J. Carneiro, J. Martins, M.F. Costa, R. Vassen, D. Stoever, Characterization of thermal barrier coatings with a gradient in porosity, Surface and Coatings Technology 195 (2005) 245–251.

[20] A. Nusair Khan, I.N. Qureshi, Microstructural evaluation of ZrO_2–MgO coatings, Journal of Materials Processing Technology 209 (2009) 488–496.

[21] A. Nusair Khan, S.H. Khan, Farhad Ali, M.A. Iqbal, Evaluation of ZrO_2–24MgO ceramic coating by eddy current method, Computational Materials Science 44 (2009) 1007–1012.

[22] S.H. Cho, S.B. Park, J.H. Lee, J.M. Hur, H.S. Lee, Hot corrosion behavior of ZrO_2–MgO coatings in LiCl–Li_2O molten salt, Materials Chemistry and Physics 131 (2012) 743–751.

[23] C. Zhu, P. Li, A. Javed, G.Y. Liang, P. Xiao, An investigation on the microstructure and oxidation behavior of laser remelted air plasma sprayed thermal barrier coatings, Surface and Coatings Technology 206 (2012) 3739–3746.

[24] R. Eriksson, H. Brodin, S. Johansson, L. Östergren, X.-H. Li, Fractographic and microstructural study of isothermally and cyclically heat treated thermal barrier coatings, Surface and Coatings Technology xxx (2012) (xxx–xxx).

[25] J.M. Drexler, C.-H. Chen, A.D. Gledhill, K. Shinoda, Plasma sprayed gadolinium zirconate thermal barrier coatings that are resistant to damage by molten Ca–Mg–Al-silicate glass, Surface and Coatings Technology 206 (19/20) (2012) 3911–3916.

[26] M.R. Begley, H.N.G. Wadley, Delamination resistance of thermal barrier coatings containing embedded ductile layers, Acta Materialia 60 (2012) 2497–2508.

[27] A.M. Khoddami, A. Sabour, S.M.M. Hadavi, Microstructure formation in thermally-sprayed duplex and functionally graded NiCrAlY/yttria-stabilized zirconia coatings, Surface and Coatings Technology 201 (2007) 6019–6024.

[28] A. Kawasaki, R. Watanabe, Thermal fracture behavior of metal/ceramic functionally graded materials, Engineering Fracture Mechanics 69 (2002) 1713–1728.

[29] K.A. Khor, Y.W. Gu, Effects of residual stress on the performance of plasma sprayed functionally graded ZrO_2/NiCoCrAlY coatings, Materials Science and Engineering: A 277 (2000) 64–76.

[30] U. Schulz, M. Peters, Fr-W. Bach, G. Tegeder, Graded coatings for thermal, wear and corrosion barriers, Materials Science and Engineering: A 362 (2003) 61–80.

[31] K.A. Khor, Z.L. dong, Y.W. Gu, Plasma sprayed functionally graded thermal barrier coatings, Materials Letters 38 (1999) 437–444.

[32] J.-Y. Kwon, S.-I. Jung, S.Y. Lee, P.H. Lee, J.H. Lee, Y.G. Jung, U. Paik, H. Cho, J.C. Chang, Interfacial stability and contact damage resistance by incorporating buffer layer in thermal barrier coatings, Progress in Organic Coatings 67 (2010) 95–101.

[33] H. TsuKamoto, Design of functionally graded thermal barrier coatings based on a nonlinear micromechanical approach, Computational Materials Science 50 (2010) 429–436.

[34] S.C. Joshi, H.W. Ng, Optimizing functionally graded nickel–zirconia coating profiles for thermal stress relaxation, Simulation Modelling Practice and Theory 19 (2011) 586–598.

[35] X.C. Zhang, B.S. Xu, H.D. Wang, Y. Jiang, Y.X. Wu, Application of functionally graded interlayer on reducing the residual stress discontinuities at interfaces within a plasma-sprayed thermal barrier coating, Surface and Coatings Technology 201 (2007) 5716–5719.

[36] Special Metals Product Handbook of High-Performance Alloys, Publication Number SMC-080, Special Metals Corporation, USA, 2004.

[37] S. Ahmaniemi, P. Vuoristo, T. Mantyla, F. Cernuschi, L. Lorenzoni, Modified thick thermal barrier coatings: thermophysical characterization, Journal of the European Ceramic Society 24 (2004) 2669–2679.

[38] J. Pina, A. Dias, J.L. Lebrun, Study by X-ray diffraction and mechanical analysis of the residual stress generation during thermal spraying, Materials Science and Engineering: A 347 (2003) 21–31.

[39] L. Pawlowski, The Science and Engineering of Thermal Spray Coatings, second ed., John Wiley & Sons, England, 2008.

[40] S. Widjaja, A.M. Limarga, T.H. Yip, Modeling of residual stresses in a plasma-sprayed zirconia/alumina functionally graded-thermal barrier coating, Thin Solid Films 434 (2003) 216–227.
[41] X.C. Zhang, B.S. Xu, H.D. Wang, Y.X. Wu, Modeling of the residual stresses in plasma-spraying functionally graded ZrO2/NiCoCrAlY coatings using finite element method, Materials and Design 27 (2006) 308–315.
[42] K.A. Khor, Z.L. Dong, Y.W. Gu, Influence of oxide mixtures on mechanical properties of plasma sprayed functionally graded coating, Thin Solid Films 368 (2000) 86–92.